Inorg. Chem. **2007**, *46*, 8763–8770

Two Iron-Containing Tungstogermanates: $[K(H_2O)(\beta\text{-}Fe_2GeW_{10}O_{37}(OH))(\gamma\text{-}GeW_{10}O_{36})]^{12-}$ and $[\{\beta\text{-}Fe_2GeW_{10}O_{37}(OH)_2\}_2]^{12-}$

Nadeen H. Nsouli,[†] Sib Sankar Mal,[†] Michael H. Dickman,[†] Ulrich Kortz,*[,†] Bineta Keita,[‡] Louis Nadjo,[‡] and Juan M. Clemente-Juan[§,||]

Jacobs University Bremen, School of Engineering and Science, P.O. Box 750 561, 28725 Bremen, Germany, Laboratoire de Chimie Physique, UMR 8000, CNRS, Equipe d'Electrochimie et Photoélectrochimie, Université Paris-Sud, Bâtiment 350, 91405 Orsay Cedex, France, Instituto de Ciencia Molecular, Universidad de Valencia, Poligono La Coma s/n, 46980 Paterna, Spain, and Fundació General de la Universidad de Valencia

Received June 1, 2007

Interaction of the dilacunary polyanion precursor $[\gamma\text{-}GeW_{10}O_{36}]^{8-}$ with Fe^{3+} ions in aqueous buffer medium (pH 4.8) results in the formation of two dimeric tungstogermanates depending on the reactant ratios. When using an Fe^{3+} to $[\gamma\text{-}GeW_{10}O_{36}]^{8-}$ ratio of 1:1, the asymmetric anion $[K(H_2O)(\beta\text{-}Fe_2GeW_{10}O_{37}(OH))(\gamma\text{-}GeW_{10}O_{36})]^{12-}$ (**1**) is formed, whereas $[\{\beta\text{-}Fe_2GeW_{10}O_{37}(OH)_2\}_2]^{12-}$ (**2**) is formed when using a ratio of 2:1. Single-crystal X-ray analyses were carried out on $Cs_3K_9[K(H_2O)(\beta\text{-}Fe_2GeW_{10}O_{37}(OH))(\gamma\text{-}GeW_{10}O_{36})]\cdot 19H_2O$ (**CsK-1**), which crystallizes in the triclinic system, space group $P\bar{1}$, $a = 11.4547(2)$, $b = 19.9181(5)$, $c = 21.0781(6)$ Å, $\alpha = 66.7977(12)$, $\beta = 89.1061(12)$, $\gamma = 84.4457(11)°$, and $Z = 2$ and on $Cs_7K_4Na[\{\beta\text{-}Fe_2GeW_{10}O_{37}(OH)_2\}_2]\cdot 39H_2O$ (**CsKNa-2**), which crystallizes in the monoclinic system, space group $C2/m$, $a = 32.7569(13)$, $b = 12.2631(5)$, $c = 14.2895(5)$ Å, $\beta = 104.135(2)°$, and $Z = 2$. Polyanion **1** consists of $(\beta\text{-}Fe_2GeW_{10}O_{37})$ and $(\gamma\text{-}GeW_{10}O_{36})$ units linked via two Fe–O–W bridges and a central potassium ion. Two equivalent FeO_6 octahedra complete the belt of the β-Keggin unit and link to the $(\gamma\text{-}GeW_{10}O_{36})$ fragment. On the other hand, **2** consists of two $\{\beta\text{-}Fe_2GeW_{10}O_{37}(OH)_2\}$ units with four bridging hydroxo groups linking the four Fe^{3+} ions, forming an eight-membered ring. The magnetic properties of **CsK-1** and **CsKNa-2** have been studied by magnetic susceptibility and magnetization measurements and fitted according to an isotropic exchange model. Both polyanions **1** and **2** exhibit diamagnetic ground states with a small amount of paramagnetic impurity. Electrochemistry studies on **1** and **2** were carried out in a pH 5 acetate medium. The two polyanions have in common the simultaneous reduction of all of their Fe^{3+} centers. This observation suggests the existence of identical or almost-identical influences on these centers and their equivalence, especially in the reduced state. Controlled potential coulometry results indicate the presence of two Fe^{3+} centers in **1** and four in **2**. The splitting of the tungsten wave of **1** compared to the single tungsten wave of **2** is attributed to a difference in acid–base properties of the polyanions. Voltammetric peak-potential shifts as a function of pH were studied in the case of **2**.

Introduction

Polyoxometalates (POMs), frequently referred to as molecular metal-oxide fragments, have attracted much attention in recent years. These inorganic anions form a large class of cage complexes based on early d-block metals in high oxidation states (e.g., W^{6+}, Mo^{6+}, V^{5+}) octahedrally coordinated by six oxo-ligands.[1–4] Sharing of these MO_6 octa-

* To whom correspondence should be addressed. E-mail: u.kortz@jacobs-university.de, Fax: (+49)421-200 3229.
[†] School of Engineering and Science, Jacobs University Bremen.
[‡] Equipe d'Electrochimie et Photoélectrochimie, Université Paris-Sud.
[§] Instituto de Ciencia Molecular, Universidad de Valencia.
[||] Fundació General de la Universidad de Valencia.

(1) Berzelius, J. *Poggendorf's Ann. Phys.* **1826**, *6*, 369.
(2) (a) Keggin, J. F. *Nature* **1933**, *131*, 908. (b) Keggin, J. F. *Proc. R. Soc. London, Ser. A* **1934**, *144*, 75.
(3) Pope, M. T. *Heteropoly and Isopoly Oxometalates*; Springer: Berlin 1983.

10.1021/ic701084x CCC: $37.00
Published on Web 09/22/2007

hedra via corners or edges results in a large structural variety. Also, one or more tetrahedral or trigonal-pyramidal hetero groups are frequently encountered. POMs are usually synthesized in aqueous, acidic medium, but the mechanism of formation is not yet well understood and is commonly described as self-assembly. Therefore, the design of discrete, molecular POMs with novel structures remains a challenge for synthetic chemists. One goal in POM synthesis is the incorporation of different functional units (e.g., transition metals, lanthanides, and organometallic entities) into the lacunary polyanion precursors.

POMs have many interesting properties that can be systematically modified, for example, shape, size, composition, charge, redox potentials, solubility, and reactivity. Therefore, this class of compounds is of interest in many different areas of science and technology. Beyond the traditional interest in catalysis,[5] POMs are currently being investigated in various fields including materials science,[6] molecular magnetism,[7] medicinal chemistry,[8] photochemistry,[9] and in electron-transfer processes.[10]

From the magnetism point of view, incorporation of more and more exchange-coupled paramagnetic transition-metal ions into these POM frameworks may result in molecules with high-spin ground states, large spin anisotropies, hysteresis, etc.[11] Such materials are ultimately of technical interest in the areas of data storage materials, magnetic switches, and so on.

Tungstosilicates and tungstogermanates represent a large and well-known subclass of POMs, and, in particular, many transition-metal-substituted tungstosilicates have been reported.[12] Iron-containing POMs possess many catalytic applications due to the easily accessible $Fe^{2+/3+}$ redox couple and magnetic applications due to the large number of unpaired electrons in high-spin Fe^{3+}.[13] Up to now, many Fe^{3+}-containing POMs have been reported, such as Hill's dimeric tungstosilicates $[(\alpha\text{-}SiFe_3W_9(OH)_3O_{34})_2(OH)_3]^{11-}$ and $[(\alpha\text{-}Si(FeOH_2)_2FeW_9(OH)_3O_{34})_2]^{8-}$, Tézé's $[\{\alpha\text{-}SiW_{10}O_{37}Fe_2(OH)_2\}_2]^{12-}$,[14] the Weakley-type sandwich POMs including mixed-metal derivatives (e.g., $[Fe_4(H_2O)_2(B\text{-}\alpha\text{-}PW_9O_{34})_2]^{6-}$ and $[Mn_2(H_2O)_2Fe_2(B\text{-}\alpha\text{-}P_2W_{15}O_{56})_2]^{14-}$),[15] the Krebs-type derivatives $[Fe_4(H_2O)_{10}(\beta\text{-}XW_9O_{33})_2]^{n-}$ ($n = 6$, X = As^{III}, Sb^{III}; $n = 4$, X = Se^{IV}, Te^{IV}),[16] the Knoth-type tungstogermanate $[Fe_6(OH)_3(A\text{-}\alpha\text{-}GeW_9O_{34}(OH)_3)_2]^{11-}$,[17] the monomeric Keggin-type species $[\gamma(1,2)\text{-}SiW_{10}\{Fe(OH_2)\}_2O_{38}]^{6-}$ and $[\beta\text{-}SiFe_2W_{10}O_{36}(OH)_2(H_2O)Cl]^{5-}$,[18] and the dimeric tungstophosphate $[Fe_4(OH)_4(PW_{10}O_{37})_2]^{10-}$.[19]

Recently, our group reported the synthesis and structural characterization of the dilacunary decatungstogermanate $[\gamma\text{-}GeW_{10}O_{36}]^{8-}$.[20] To date, only a few derivatives of this polyanion precursor have been reported.[21] Here, we report on the synthesis, structure, electrochemistry, and magnetism of two novel Fe^{3+}-containing tungstogermanates.

Experimental Section

Synthesis. $K_8[\gamma\text{-}GeW_{10}O_{36}]\cdot 6H_2O$ was synthesized according to the published procedure, and its identity was confirmed by infrared spectroscopy.[20] All of the other reagents were used as purchased without further purification.

$Cs_3K_9[K(H_2O)(\beta\text{-}Fe_2GeW_{10}O_{37}(OH))(\gamma\text{-}GeW_{10}O_{36})]\cdot 19H_2O$ (CsK-1). A 0.050 g (0.019 mmol) sample of $FeCl_3\cdot 6H_2O$ was dissolved in 20 mL 1M HOAc/KOAc buffer (pH 4.8), and then 0.50 g (0.017 mmol) of $K_8[\gamma\text{-}GeW_{10}O_{36}]\cdot 6H_2O$ was added. This

(4) (a) Pope, M. T.; Müller, A. *Angew. Chem., Int. Ed. Engl.* **1991**, *30*, 34. (b) Pope, M. T.; Müller, A. *Polyoxometalates: From Platonic Solids to Anti Retroviral Activity*; Kluwer: Dordrecht, The Netherlands, 1994. (c) Hill, C. L.; Prosser-McCartha, C. M. *Coord. Chem. Rev.* **1995**, *143*, 407. (d) *Chem. Rev.* **1998**, *98*, 1−389 (Special Thematic Issue on Polyoxometalates). (e) Pope, M. T.; Müller, A. *Polyoxometalate Chemistry: From Topology via Self-Assembly to Applications*; Kluwer: Dordrecht, The Netherlands, 2001. (f) *Polyoxometalate Chemistry for Nano-Composite Design*; Yamase, T., Pope, M. T., Eds.; Kluwer: Dordrecht, The Netherlands, 2002. (g) Pope, M. T. *Comput. Coord. Chem. II* **2003**, *4*, 635. (h) Hill, C. L. *Comput. Coord. Chem. II* **2003**, *4*, 679. (i) Borrás-Almenar, J. J.; Coronado, E.; Müller, A.; Pope, M. T. *Polyoxometalate Molecular Science*; Kluwer: Dordrecht, The Netherlands, 2004.

(5) (a) Kozhenvnikov, I. V. *Chem. Rev.* **1998**, *98*, 171. (b) Mizuno, N.; Misono, M. *Chem. Rev.* **1998**, *98*, 199. (c) Sadakane, M.; Steckhan, E. *Chem. Rev.* **1998**, *98*, 219. (c) Okun, N.; Anderson, T.; Hill, C. *J. Am. Chem. Soc.* **2003**, *125*, 3194.

(6) Coronado, E.; Gómez-García, C. J. *Chem. Rev.* **1998**, *98*, 273.

(7) Müller, A.; Peters, F.; Pope, M. T.; Gatteschi, D. *Chem. Rev.* **1998**, *98*, 239.

(8) Schinazi, R. F. *Chem. Rev.* **1998**, *98*, 327.

(9) (a) Carls, J.; Argitis, P.; Heller, A. *Electrochem. Soc.* **1992**, *139*, 786. (b) Yamase, T.; Ohtaka, K. *J. Chem. Soc., Dalton Trans.* **1994**, 2599.

(10) Weinstock, I. A. *Chem. Rev.* **1998**, *98*, 113.

(11) (a) Bassil, B. S.; Nellutla, S.; Kortz, U.; Stowe, A. C.; van Tol, J.; Dalal, N. S.; Keita, B.; Nadjo, L. *Inorg. Chem.* **2005**, *44*, 2659−2665. (b) Kortz, U.; Nellutla, S.; Stowe, A. C.; Dalal, N. S.; Rauwald, U.; Danquah, W.; Ravot, D. *Inorg. Chem.* **2004**, *43*, 2308. (c) Kortz, U.; Nellutla, S.; Stowe, A. C.; Dalal, N. S.; van Tol, J.; Bassil, B. S. *Inorg. Chem.* **2004**, *43*, 144. (d) Stowe, A. C.; Nellutla, S.; Dalal, N. S.; Kortz, U. *Eur. J. Inorg. Chem.* **2004**, 3792. (e) Tasiopoulos, A. J.; Vinslava, A.; Wernsdorfer, W.; Abboud, K. A.; Christou, G. *Angew. Chem., Int. Ed.* **2004**, *43*, 2117.

(12) (a) Tézé, A.; Hervé, G. *Inorg. Synth.* **1990**, *27*, 85. (b) Bassil, B. S.; Dickman, M. H.; Kortz, U. *Inorg. Chem.* **2006**, *45*, 2394. (c) Bassil, B. S.; Kortz, U.; Tigan, A. S.; Clemente-Juan, J. M.; Keita, B.; de Oliveira, P.; Nadjo, L. *Inorg. Chem.* **2005**, *44*, 9360. (d) Bi, L.-H.; Kortz, U.; Dickman, M. H.; Keita, B.; Nadjo, L. *Inorg. Chem.* **2005**, *44*, 7485. (e) Kortz, U.; Nellutla, S.; Stowe, A. C.; Dalal, N. S.; Rauwald, U.; Danquah, W.; Ravot, D. *Inorg. Chem.* **2004**, *43*, 2308. (f) Bi, L.-H.; Kortz, U.; Nellutla, S.; Stowe, A. C.; Dalal, N. S.; Keita, B.; Nadjo, L. *Inorg. Chem* **2005**, *44*, 896.

(13) (a) Bonchio, M.; Carraro, M.; Sartorel, A.; Scorrano, G.; Kortz, U. *J. Mol. Catal. A: Chem.* **2006**, *251*, 93. (b) Nishiyama, Y.; Nakagawa, Y.; Mizuno, N. *Angew. Chem., Int. Ed.* **2001**, *40*, 3639.

(14) (a) Anderson, T.; Neiwert, W.; Hardcastle, K.; Hill, C. *Inorg. Chem.* **2004**, *43*, 7353. (b) Tézé, A.; Vaissermann, J. *C. R. Acad. Sci., Ser. IIc: Chim.* **2000**, *3*, 101.

(15) (a) Anderson, T. M.; Zhang, X.; Hardcastle, K. I.; Hill, C. L. *Inorg. Chem.* **2002**, *41*, 2477. (b) Anderson, T. M.; Hardcastle, K. I.; Okun, N.; Hill, C. L. *Inorg. Chem.* **2001**, *40*, 6418. (c) Zhang, X.; Chen, Q.; Duncan, D. C.; Lachicotte, R. J.; Hill, C. L. *Inorg. Chem.* **1997**, *36*, 4381. (d) Zhang, X.; Chen, Q.; Duncan, D. C.; Campana, C. F.; Hill, C. L. *Inorg. Chem.* **1997**, *36*, 4208.

(16) Kortz, U.; Savelieff, M. G.; Bassil, B. S.; Keita, B.; Nadjo, L. *Inorg. Chem.* **2002**, *41*, 783.

(17) Bi, L.-H.; Kortz, U.; Nellutla, S.; Stowe, A. C.; Dalal, N. S.; Keita, B.; Nadjo, L. *Inorg. Chem.* **2005**, *44*, 896.

(18) (a) Botar, B.; Geletii, Y.; Kögerler, P.; Musaev, D.; Morokuma, J.; Weinstock, I.; Hill, C. *Dalton Trans.* **2005**, 2017. (b) Nozaki, C.; Kiyoto, I.; Minai, Y.; Misono, M.; Mizuno, N. *Inorg. Chem.* **1999**, *38*, 5724.

(19) Li, M.-X.; Jin, S.-L.; Liu, H.-Z.; Xie, G.-Y.; Chen, M.-Q.; Xu, Z.; You, X.-Z. *Polyhedron* **1998**, *17*, 3721.

(20) Nsouli, N. H.; Bassil, B. S.; Dickman, M. H.; Kortz, U.; Keita, B.; Nadjo, L. *Inorg. Chem.* **2006**, *45*, 3858.

(21) (a) Bi, L.-H.; Chubarova, E. V.; Nsouli, N. H.; Dickman, M. H.; Kortz, U.; Keita, B.; Nadjo, L. *Inorg. Chem.* **2006**, *45*, 8575. (b) We have already isolated several other transition-metal-containing derivatives of $[\gamma\text{-}GeW_{10}O_{36}]^{8-}$, for example $[Cu_3(H_2O)(B\text{-}\beta\text{-}GeW_9O_{33}(OH))(B\text{-}\beta\text{-}GeW_8O_{29}(OH))]^{10-}$, $[\{\beta\text{-}GeNi_2W_{10}O_{36}(OH)_2(H_2O)\}_2]^{12-}$, and $\{[\beta\text{-}GeW_{11}MnO_{39}]^{6-}\}_\infty$. These results will be published in the near future elsewhere.

solution was heated to 40 °C for 30 min, cooled to room temperature, and filtered. Then, 0.5 mL of 1M CsCl solution was added. Slow evaporation at room temperature led to yellow-green crystals suitable for X-ray diffraction within 1 week. The product was isolated by filtration and then air-dried (yield 0.050 g, 94%). IR: 946 (s), 877 (m), 803 (s), 734 (s), 704 (s), 648 (sh), 530 (m), 461 (m) cm^{-1}. Anal. Calcd for **CsK-1**: Cs, 6.4; K, 6.2; W, 58.7; Fe, 1.8; Ge, 2.3. Found: Cs, 6.0; K, 6.3; W, 57.2; Fe, 1.8; Ge, 2.3.

$Cs_7K_4Na[\{\beta\text{-}Fe_2GeW_{10}O_{37}(OH)_2\}_2]\cdot 39H_2O$ (CsKNa-2). A 0.10 g (0.037 mmol) sample of $FeCl_3\cdot 6H_2O$ was dissolved in 20 mL of 1M HOAc/NaOAc buffer (pH 4.8), and then 0.50 g (0.017 mmol) of $K_8[\gamma\text{-}GeW_{10}O_{36}]\cdot 6H_2O$ was added. This solution was heated to 45 °C for 30 min, cooled to room temperature, and filtered. Then, 0.75 mL of 1M CsCl was added. Slow evaporation at room temperature led to orange crystals suitable for X-ray diffraction within 1 week. The product was isolated by filtration and then air-dried (yield 0.045 g, 74%). IR: 946 (m), 873 (m), 802 (s), 758 (s), 650 (m), 522 (m), 458 (m), 439 (sh) cm^{-1}. Anal. Calcd for **CsKNa-2**: Cs, 13.1; K, 2.2; Na, 0.3; W, 51.7; Fe, 3.1; Ge, 2.0. Found: Cs, 12.8; K, 2.0; Na, 0.4; W, 50.2; Fe, 3.1; Ge, 1.9.

Elemental analyses for **CsK-1** and **CsKNa-2** were performed by Gesellschaft für Laboruntersuchungen mbH, Wesseling bei Köln, Germany. Infrared spectra were recorded on KBr pellets using a Nicolet Avatar spectrophotometer. Thermogravimetric analyses were carried out on a TA Instruments SDT Q600 thermobalance with a 100 mL/min flow of nitrogen; the temperature was ramped from 20 to 800 °C at a rate of 2 °C/min.

X-ray Crystallography. A crystal of **CsK-1** was picked from the solution, mounted on a glass fiber, and coated with epoxy glue for data collection at room temperature. A crystal of **CsKNa-2** was picked from solution and mounted in a Hampton cryoloop using light oil for data collection at −100 °C. Indexing and data collection for both were performed on a Bruker D8 SMART APEX II CCD diffractometer with kappa geometry and Mo Kα radiation (graphite monochromator, $\lambda = 0.71073$ Å). Data integration was performed using *SAINT*.[22] Routine Lorentz and polarization corrections were applied. Multiscan absorption corrections were performed using *SADABS*.[23] Direct methods (*SHELXS97*) successfully located the tungsten atoms, and successive Fourier syntheses (*SHELXL97*) revealed the remaining atoms.[24] Refinements were full-matrix least-squares against $|F|^2$ using all of the data. The cations and waters of hydration were modeled with varying degrees of occupancy. In contrast to the elemental analysis of **CsKNa-2**, which shows seven cesium, four potassium, and one sodium cation, only four cesium cation sites (on special positions, amounting to eight positive charges) were found in the X-ray model. It is not unusual for the X-ray models of polytungstates to contain fewer cations than found by elemental analysis, and it is possible that the cesium sites also contain disordered potassium atoms. However, no attempt was made to model the cation sites as disordered cesium/potassium/sodium atoms. In the final refinement, all of the non-disordered heavy atoms (tungsten, cesium, germanium, and iron) were refined anisotropically, whereas the oxygen atoms and disordered cations were refined isotropically. No hydrogen atoms were included in the models. Crystallographic data are summarized in Table 1.

UV−Visible Spectroscopy. Pure water was used throughout. It was obtained by passing through a RiOs 8 unit followed by a Millipore-Q Academic purification set. All of the reagents were of high-purity grade and were used as purchased without further purification. The UV−visible spectra were recorded on a PerkinElmer Lambda 19 spectrophotometer on 2.5×10^{-4} M solutions of **1** and **2**. Matched 1.000 cm optical-path quartz cuvets were used. The following media are useful for the present study: 0.4 M CH_3CO_2Na/CH_2ClCO_2H, pH = 3; 0.4M CH_3CO_2Na/CH_3CO_2H, pH = 4 and 5.

Table 1. Crystal Data and Structure Refinement for $Cs_3K_9[K(H_2O)(\beta\text{-}Fe_2GeW_{10}O_{37}(OH))(\gamma\text{-}GeW_{10}O_{36})]\cdot 19H_2O$ (**CsK-1**) and $Cs_7K_4Na[\{\beta\text{-}Fe_2GeW_{10}O_{37}(OH)_2\}_2]\cdot 39H_2O$ (**CsKNa-2**)

	CsK−1	CsKNa−2
emp formula	$H_{41}Cs_3Fe_2Ge_2K_{10}O_{94}W_{20}$	$H_{82}Cs_7Fe_4Ge_2K_4NaO_{117}W_{20}$
fw	6268.7	7109.7
space group	$P\bar{1}$	$C2/m$
a (Å)	11.4547(2)	32.7569(13)
b (Å)	19.9181(5)	12.2631(5)
c (Å)	21.0781(6)	14.2895(5)
α (deg)	66.7977(12)	90
β (deg)	89.1061(12)	104.135(2)
γ (deg)	84.4457(11)	90
vol ($Å^3$)	4398.04(18)	5566.3(4)
Z	2	2
temp (°C)	25	−100
wavelength (Å)	0.71073	0.71073
d_{calcd} (mg/m^3)	4.518	4.321
abs coeff (mm^{-1})	28.522	24.459
R [$I > 2\sigma(I)$][a]	0.051	0.096
R_w (all data)[b]	0.163	0.288

[a] $R = \sum||F_o| - |F_c||/\sum|F_o|$. [b] $R_w = [\sum w(F_o^2 - F_c^2)^2/\sum w(F_o^2)^2]^{1/2}$.

Electrochemical Experiments. The solutions were deaerated thoroughly for at least 30 min with pure argon and kept under a positive pressure of this gas during the experiments. The source, mounting, and polishing of the glassy carbon (GC, Tokai, Japan) electrodes has been described.[25] The glassy carbon samples had a diameter of 3 mm. The electrochemical setup was an EG & G 273 A driven by a PC with the M270 software. Potentials are quoted against a saturated calomel electrode. The counter electrode was a platinum gauze of large surface area. All of the experiments were performed at room temperature.

Results and Discussion

Synthesis and Structure. The reaction of $FeCl_3\cdot 6H_2O$ with $K_8[\gamma\text{-}GeW_{10}O_{36}].6H_2O$ in ratios of 1:1 and 2:1, respectively, in sodium acetate buffer (pH 4.8) results in two different novel, dimeric tungstogermanates depending on the reactant ratios. Using an Fe^{3+} to $[\gamma\text{-}GeW_{10}O_{36}]^{8-}$ ratio of 1:1, $[K(H_2O)(\beta_{22}\text{-}Fe_2GeW_{10}O_{37}(OH))(\gamma\text{-}GeW_{10}O_{36})]^{12-}$ (**1**) is formed, whereas $[\{\beta_{22}\text{-}Fe_2GeW_{10}O_{37}(OH)_2\}_2]^{12-}$ (**2**) is formed when using a ratio of 2:1.

Polyanion **1** has a rather unusual and asymmetric structure, consisting of two different Keggin moieties. The di-iron-containing decatungstogermanate unit ($\beta_{22}\text{-}Fe_2GeW_{10}O_{37}$) and the well-known dilacunary decatungstogermanate ($\gamma\text{-}GeW_{10}O_{36}$) are linked via two Fe−O−W bridges and a potassium cation, resulting in an assembly with C_s symmetry (Figure 1). The two corner-sharing FeO_6 octahedra complete the belt of the β_{22}-Keggin fragment and are the linkers to the ($\gamma\text{-}GeW_{10}O_{36}$) unit. Bond valence sum (BVS) calculations[26] confirm the monoprotonation of the μ_2-oxo ligand

(22) *SAINT*; Bruker Analytical X-ray Systems, Inc.: Madison, WI, 1998.
(23) Sheldrick, G. M. *SADABS*, University of Göttingen: Göttingen, Germany, 2003.
(24) (a) G. M. Sheldrick, *SHELXS-97, Program for Solution of Crystal Structures*; University of Göttingen: Göttingen, Germany, 1997. (b) G. M. Sheldrick, *SHELXL-97, Program for Refinement of Crystal Structures*; University of Göttingen: Göttingen, Germany, 1997.
(25) Keita, B.; Nadjo, L. *J. Electroanal. Chem*. **1988**, *243*, 87.
(26) Brown, I. D.; Altermatt, D. *Acta. Crystallogr. B* **1985**, *41*, 244.

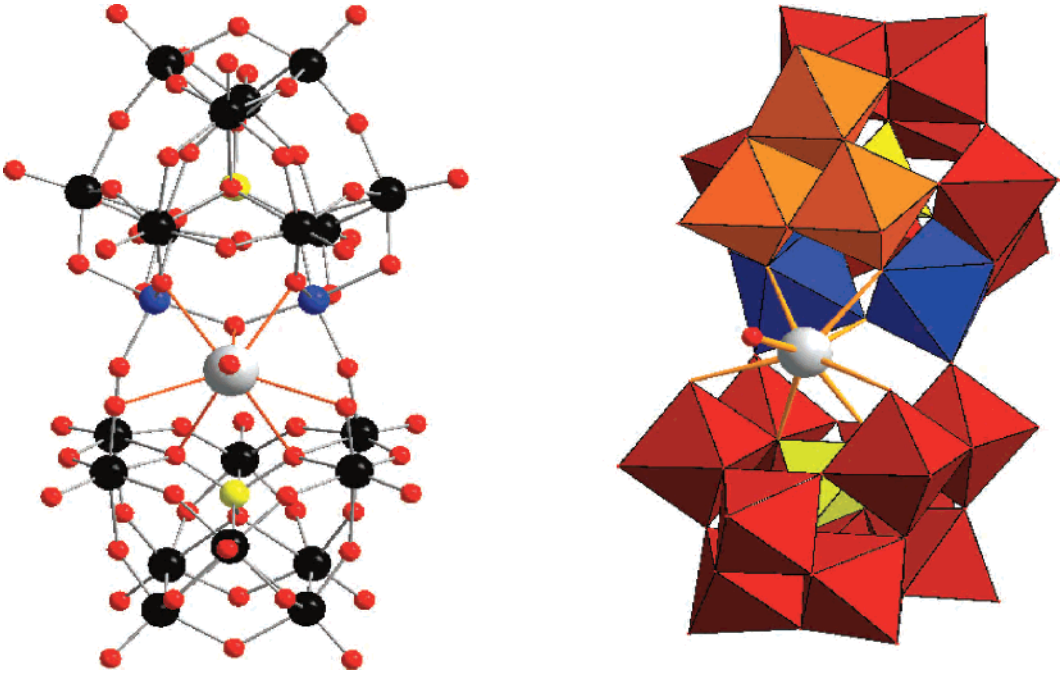

Figure 1. Ball-and-stick (left) and polyhedral (right) representations of **1**. Color code: The balls represent iron (blue), tungsten (black), germanium (yellow), oxygen (red), and potassium (gray); the polyhedra represent FeO_6 (blue), GeO_4 (yellow), WO_6 (red), and WO_6 of the β-rotated triad (orange).

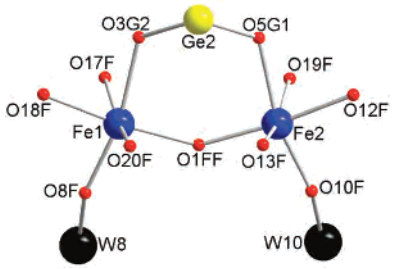

Figure 2. Ball-and-stick representation of the iron coordination spheres in **1**. Bond lengths (Å): W(8)−O(8F), 1.828(16); W(10)−O(10F), 1.807(16); Fe(1)−O(8F), 1.927(16); Fe(1)−O(1FF), 1.996(15); Fe(1)−O(20F), 1.977(15); Fe(1)−O(18F), 2.003(16); Fe(1)−O(17F), 1.807(16); Fe(1)−O(3G2), 2.171(14); Fe(2)−O(10F), 1.913(17); Fe(2)−O(1FF), 1.988(14); Fe(2)−O(13F), 1.979(15); Fe(2)−O(19F), 2.016(16); Fe(2)−O(12F), 2.016(14); Fe(2)−O(5G1), 2.143(15); Angles (°): Fe(2)−O(1FF)−Fe(1), 38.8(8); W(8)−O(8F)−Fe(1), 148.2(9); W(10)−O(10F)−Fe(2), 151.5(10).

(O1FF) bridging the two iron atoms, and the fact that the terminal ligand (O19W) of the K^+ ion located in the center of **1** is actually a water molecule. The Fe−O bond distances of all μ_2-oxo bridges range from 1.913(17) to 2.016(16) Å, whereas the Fe−O bonds to μ_4-oxo bridges are somewhat longer (2.171(14) and 2.143(15) Å, respectively; Figure 2). The oxygen atoms O8F and O10F bridge the iron centers of the (β-$Fe_2GeW_{10}O_{37}$) unit to W8 and W10 of the (γ-$GeW_{10}O_{36}$) unit, with an average W−O bond distance of 1.818(16) Å, forming angles of 148.2(9) and 151.5(10)°, respectively. This average W−O distance is slightly longer than the corresponding average W−O distance (1.755(19) Å) on the adjacent WO_6 octahedra (W7 and W9) of the (γ-$GeW_{10}O_{36}$) unit. The hydroxo group O1FF links the two iron atoms of the (β-$Fe_2GeW_{10}O_{37}$) fragment with an Fe−OH−Fe angle of 138.8(8)°. The K^+ cation in the center of the anion is eight-coordinate with a K−OH_2 bond distance of 2.77(4) Å, the others ranging from 2.792(16) to 3.052(16) Å.

Polyanion **1** is an example of a POM dimer in which each half-unit could in theory be isolated, which is in contrast with the familiar Weakley (e.g., $[Fe_4(H_2O)_2(B\text{-}\alpha\text{-}PW_9O_{34})_2]^{6-}$) and Krebs-type (e.g., $[Fe_4(H_2O)_{10}(B\text{-}\beta\text{-}As^{III}W_9O_{33})_2]^{6-}$) dimers.[15c,16] The bridging mode of **1** is unusual in that most such Fe^{3+}-containing POMs form dimers through Fe−O−Fe bonds.[14] The only other dimeric structure of this type of which we are aware that is linked by Fe−O−W bridges is $[(\alpha\text{-}Si(FeOH_2)_2FeW_9(OH)_3O_{34})_2]^{8-}$.[14a] The presence of the (γ-$GeW_{10}O_{36}$) unit in a dimeric transition metal-containing POM is unprecedented. Since the first report of the precursor $[\gamma\text{-}GeW_{10}O_{36}]^{8-}$,[20] the only other structure containing the (γ-$GeW_{10}O_{36}$) fragment is $[\{Ru(C_6H_6)(H_2O)\}\{Ru(C_6H_6)\}(\gamma\text{-}GeW_{10}O_{36})]^{4-}$, a monomeric POM in which two benzene-Ru groups are grafted to the decatungstate framework.[21a]

Polyanion **2** is also a dimeric POM, but in contrast to **1**, it is composed of two identical (β_{22}-$Fe_2GeW_{10}O_{37}(OH)_2$) Keggin moieties linked via two Fe−OH−Fe bridges (Figure 3). Interestingly, **2** showed crystallographic 2/*m* symmetry, implying 50% disorder of the rotated triad in each (β_{22}-$Fe_2GeW_{10}O_{37}(OH)_2$) unit. This indicates the possible presence of two geometric isomers in the crystal studied: one with the two rotated triads on the same side of the anion (syn isomer, with C_{2v} symmetry), the other having the rotated triads on opposite sides (anti isomer, with C_{2h} symmetry), as illustrated in Figure 3.

Two corner-shared FeO_6 octahedra complete the belt of each of the two Keggin units in **2**. The linkage of the two Keggin units to each other is accomplished via two pairs of corner-shared FeO_6 octahedra (Figure 3). According to BVS

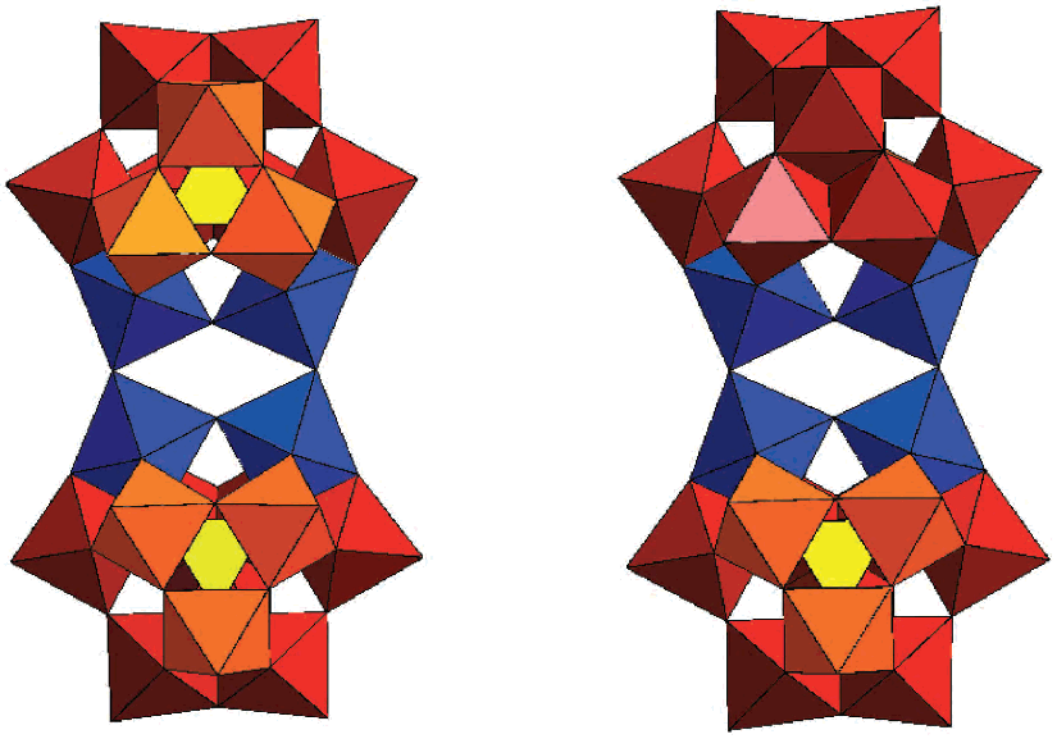

Figure 3. Polyhedral representations of the syn (left) and anti (right) geometric isomers of **2**. The color code is the same as that in Figure 1.

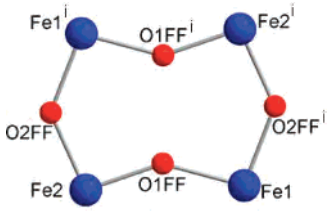

Figure 4. Ball-and-stick representation of the cyclic $Fe_4(OH)_4$ unit in **2**. Symmetry operation: $i = -x, -y, -z$.

calculations, the four Fe−O−Fe bridges O1FF, O1FF^{i}, O2FF, O2FF^{i} are all monoprotonated and thus the intra- and inter-Keggin connectivities in **2** are all via bridging hydroxo groups (Figure 4). This is in complete agreement with the two related Keggin dimers reported previously, Tézé's [{α-$SiW_{10}O_{37}Fe_2(OH)_2\}_2]^{12-}$ and Jin's [{α-$PW_{10}O_{37}Fe_2(OH)_2\}_2]^{10-}$.[14b,19] However, in contrast to **2**, the $Fe_4(OH)_4$ cycle in these two polyanions is not planar. The reason is that, in [{α-$SiW_{10}O_{37}Fe_2(OH)_2\}_2]^{12-}$ and [{α-$PW_{10}O_{37}Fe_2(OH)_2\}_2]^{10-}$, the two iron atoms are located in the corner-shared triad of the (α-$XW_{10}O_{37}$) Keggin unit, rather than in the belt, as in **2**. More precisely, [{α-$SiW_{10}O_{37}Fe_2(OH)_2\}_2]^{12-}$ has a syn configuration of the two Keggin units, whereas [{α-$PW_{10}O_{37}Fe_2(OH)_2\}_2]^{10-}$ has an anti configuration.

We also performed thermogravimetric analyses (TGA) on both **CsK-1** and **CsKNa-2** under a N_2 atmosphere. These measurements allowed us to evaluate the thermal stability of polyanions **1** and **2** in the solid state. By using this technique we could also determine the number of water molecules of hydration. The compounds **CsK-1** and **CsKNa-2** start to lose crystal water almost instantaneously upon heating from room temperature up to around 200 °C for **CsK-1** and 400 °C for **CsKNa-2** (Figures S1 and S2).

Magnetic Susceptibility. Variable-temperature magnetic susceptibility data were collected on powder samples of **CsK-1** and **CsKNa-2** in the temperature range 2−300 K at 0.1 T.

For **CsK-1**, the product $\chi_m T$ shows a continuous decrease from 5.29 emu·K/mol at 300 K down to 0.12 at 2 K (Figure 5). This behavior suggests the presence of antiferromagnetic exchange interaction between the two Fe^{3+} ($S = {}^5/_2$) metal centers. Taking into account an isotropic exchange Hamiltonian, $H = -2J\hat{S}_1\hat{S}_2$, the best least-squares fit gives the following set of variables: $J = -14.2$ cm^{-1}, $g = 2.00$ (fixed), paramagnetic impurity 1.6% ($R = 4.7 \times 10^{-3}$).

For **CsKNa-2**, $\chi_m T$ decreases steadily and almost linearly from 4.8 at 300 K to 0.53 emu·K/mol at 4 K (Figure 6). At 4 K, the curve shows a plateau that can be attributed to a diamagnetic ground state for **2** with a small amount of paramagnetic impurity. The decrease below 4 K can be ascribed to intermolecular interactions. Taking into account the local symmetry of **2**, the following isotropic Hamiltonian can be applied $\hat{H} = -2J_1(\hat{S}_1\hat{S}_2 + \hat{S}_3\hat{S}_4) - 2J_2(\hat{S}_1\hat{S}_4 + \hat{S}_2\hat{S}_3)$. The best least-squares fit gives the following set of variables: $J_1 = J_2 = -26.0$ cm^{-1}, $g = 2.00$ (fixed), paramagnetic impurity 3.8% ($R = 7.5 \times 10^{-4}$).

The exchange parameters obtained from both fittings are similar to what is expected from magnetostructural models developed for oxo-bridged Fe^{3+} dimers.[27] For the case of **1**, the Fe−O−Fe distances are 1.996(15) and 1.988(14) Å, respectively, and the bond angle is 138.8(8)°. Taking into account the magnetic correlations, the calculated exchange constant is around −22 cm^{-1}. This value is close to the experimental one. For polyanion **2**, we can observe that the

(27) Weihe, H.; Güdel, H. U. *J. Am. Chem. Soc.* **1997**, *119*, 6539.

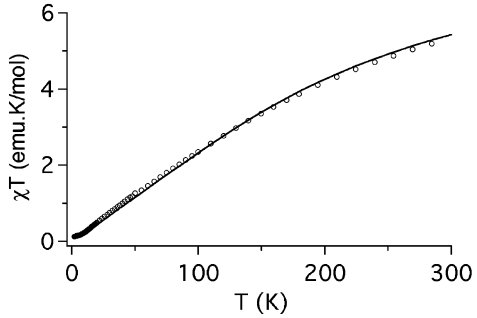

Figure 5. Thermal behavior of **CsK-1** at 0.1 T in the temperature range 2−300 K. The solid line represents the best fitting with the isotropic model used.

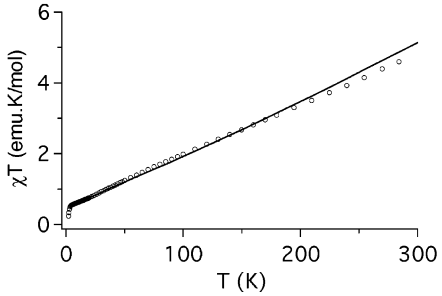

Figure 6. Thermal behavior of **CsKNa-2** at 0.1 T in the temperature range 2−300 K. The solid line represents the best fitting with the isotropic model used.

Fe−O distances are slightly shorter (1.86(3), 1.93(3), 1.94-(2), 1.94(2) Å) and the intra-Keggin Fe−O−Fe bond angle is 146.0(18)°. Hence, the expected exchange interactions should be stronger, around -40 cm^{-1}. This value fits nicely with the experimental results for **2**. Furthermore, this data is consistent with the related polyanion $[Fe_6(OH)_3(A\text{-}\alpha\text{-}GeW_9O_{34}(OH)_3)_2]^{11-}$.[17]

Electrochemistry. The stability of **1** and **2** was assessed by monitoring their respective UV−vis spectra as a function of pH over a period of at least 24 h. The stability criterion was the reproducibility of spectra with respect to absorbances and wavelengths during this period of time. Both polyanions were stable in a pH 5, acetate medium. The corresponding spectra are shown in the Supporting Information section (Figure S3). Only **2** is also stable at pH 3, as indicated by the peak not shifting. In media where **1** is not stable, the spectrum showed a gradual transformation to an ill-defined peak gradually disappearing; the spectrum broadened and lines overlapped. A complementary confirmation of the stability suggested by UV−vis spectroscopy was obtained by cyclic voltammetry, a technique for which reproducible characteristics were routinely observed for about 10 h when the relevant electrochemistry experiment was stopped. Following the results of stability tests, the two polyanions **1** and **2** were studied and compared at pH 5. Finally, the pH effect was also investigated for **2**.

Part A of Figure 7 shows the cyclic voltammogram of **2** obtained at a scan rate of 10 mV s^{-1}, in a pH 5 acetate medium. The pattern is restricted to the two waves featuring the reduction of the Fe^{3+} centers and the first W^{VI} wave, respectively. The superimposed dotted curve is helpful in assigning the various patterns observed upon the reversal of

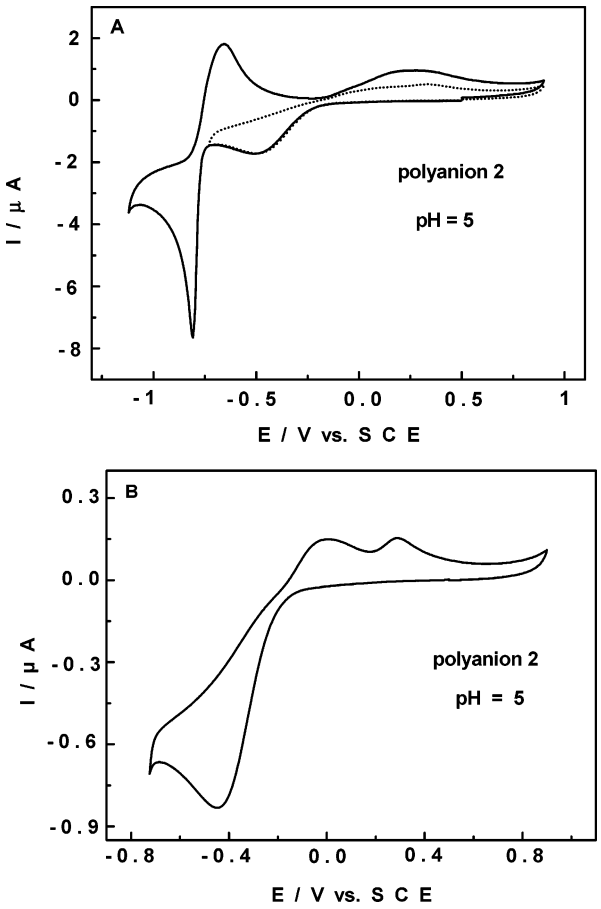

Figure 7. Cyclic voltammograms (CVs) of 2×10^{-4} M **CsKNa-2** in a pH 5 medium (0.4 M CH_3CO_2Na/CH_3CO_2H). The working electrode was glassy carbon, and the reference electrode was SCE. (A) Superposition of the CVs of **CsKNa-2**, restricted to the pattern associated with the Fe^{3+} centers (dotted-line curve) and extended to include the first W^{VI} reduction process (solid-line curve). The scan rate was 10 mV s^{-1}. (B) CV of **CsKNa-2** restricted to the pattern associated with the Fe^{3+} centers. The scan rate was 2 mV s^{-1}.

the potential scan. As expected, the W^{VI}-based wave is located at a more-negative potential than the wave attributed to the Fe^{3+} centers. This W^{VI} wave, with $E_{pc} = -0.808$ and $E_{pa} = -0.662$ V, is electrochemically quasireversible and chemically reversible, two features usually seen in related iron-containing polyanions.[12f,28] More attention was given to the reduction of the Fe^{3+} centers. A single reduction peak potential is observed at $E_{pc} = -0.484 \pm 0.005$ V (vs a saturated calomel electrode (SCE)). No splitting of this single Fe^{3+} wave was observed upon increasing the potential scan rate. After reduction of the Fe^{3+} centers, the corresponding reoxidation process is broad and shows a tendency of splitting. This trend is clearly confirmed in part B of Figure 7, which was run at a scan rate of 2 mV s^{-1}. Controlled potential coulometry with the potential set at -0.520 V versus SCE indicates the consumption of 4.06 ± 0.05 electrons per molecule. This result is consistent with the simultaneous one-electron reduction of the four Fe^{3+} centers. The characteristic blue color associated with a reduced tungsten−oxygen framework was not observed during this

(28) Anderson, T. M.; Cao, Rui.; Neiwert, W. A.; Hardcastle, K. II.; Hill, C. L.; Ammam, M.; Keita, B.; Nadjo, L. *Eur. J. Inorg. Chem.* **2005**, 1770.

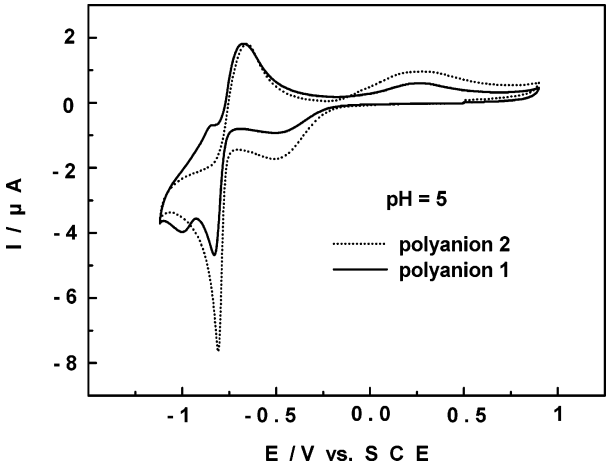

Figure 8. Superposition of cyclic voltammograms (CVs) of 2×10^{-4} M **CsK-1** (solid-line curve) and 2×10^{-4} M **CsKNa-2** (dotted-line curve), in a pH 5 medium (0.4 M CH_3CO_2Na/CH_3CO_2H). The working electrode was glassy carbon, and the reference electrode was SCE. The scan rate was 10 mV s^{-1}.

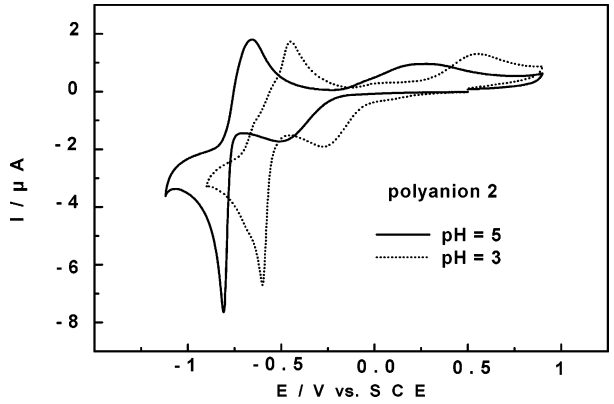

Figure 9. Superposition of cyclic voltammograms (CVs) of 2×10^{-4} M **CsKNa-2** in two different pH media: (solid-line curve) in a pH 5 medium (0.4M CH_3CO_2Na/CH_3CO_2H); (dotted-line curve) in a pH 3 medium (0.4 M CH_3CO_2Na/CH_2ClCO_2H). The working electrode was glassy carbon, and the reference electrode was SCE. The scan rate was 10 mV s^{-1}.

experiment, a behavior expected from the existence of a large potential separation between the Fe^{3+} and W^{VI}-based redox processes.

Figure 8 compares the cyclic voltammograms of **1** and **2** obtained at a scan rate of 10 mV s^{-1} in a pH 5 acetate medium. Analogies and differences between the two polyanions can be identified. The redox processes associated with the W^{VI} centers of **1** are featured by two electrochemically quasireversible and chemically reversible waves, in contrast to a single wave for **2**. In comparison with **2**, this part of the voltammetric pattern is slightly shifted in the negative potential direction ($E_{pc1} = -0.830$, $E_{pa1} = -0.666$, $E_{pc2} = -0.994$, and $E_{pa2} = -0.848$ for **1** vs $E_{pc} = -0.808$ V for **2**), and the current intensities are also smaller for **1**. This behavior is probably due to a difference in acid−base properties of the reduced forms of **1** and **2**. Such a difference is consistent with the asymmetric structure of **1** compared to the more symmetrical **2** being composed of two identical half units. The patterns associated with the redox processes of the Fe^{3+} centers in **1** and **2** are identical in potential locations and differ only in current intensities. Such an observation is expected upon considering the similar molar masses and the identical negative charges of **1** and **2**. Indeed, controlled potential coulometry with the potential set at −0.520 V versus SCE indicates the consumption of 2.05 ± 0.05 electrons per molecule, a result again consistent with the simultaneous one-electron reduction of the two Fe^{3+} centers in **1**.

In short, the simultaneous reduction of the Fe^{3+} centers is a feature shared by **1** and **2** as well as related polyanions.[12f,28] This suggests an identical or almost-identical structural/electronic influence on these iron centers, especially in the reduced state. In contrast, stepwise reduction of the Fe^{3+} centers has been reported repeatedly for sandwich-type polyanions of the Keggin and Wells−Dawson series[15d,29] and indicates some type of electronic communication between the Fe^{3+} centers. This interaction must generate and/or reinforce inequivalence among the sites, especially in the reduced state. A more-detailed discussion of this topic has been reported previously.[30]

Figure 9 shows an important pH effect on the cyclic voltammogram of **2**. Qualitatively, the entire voltammetric pattern shifted in the positive potential direction when the pH was decreased from 5 to 3, and the formerly unique tungsten wave started to split. On the basis of these two pH values, shifts of 0.104 and 0.106 V per pH unit were measured for the reduction and reoxidation waves of W^{VI}, respectively. The Fe^{3+} centers show an even-higher pH sensitivity of 0.120 for the reduction and roughly 0.150 V per pH unit for the corresponding broad composite reoxidation process. Such sensitivity of the Fe^{3+} redox processes to pH changes is not unprecedented, albeit to a lesser extent, in iron-substituted and multi-iron sandwich-type POMs.[30] Tentatively, the large sensitivity of the Fe^{3+} centers in **2** might be attributed to the four bridging hydroxo groups linking the four Fe^{3+} ions.

Conclusions

We have synthesized and structurally characterized two novel Fe^{3+}-containing tungstogermanates. The first is the asymmetric dimer $[K(H_2O)(\beta_{22}\text{-}Fe_2GeW_{10}O_{37}(OH))(\gamma\text{-}GeW_{10}O_{36})]^{12-}$ (**1**) with an unprecedented and unusual structure consisting of a (β_{22}-$Fe_2GeW_{10}O_{37}$) and a (γ-$GeW_{10}O_{36}$) unit linked via two Fe−O−W bridges, resulting in an assembly with *Cs* symmetry. A monohydrated K^+ ion is situated at the center of **1** and apparently provides additional stability to the rather-open architecture. The two iron atoms are linked to each other via a hydroxo group. The second polyanion, $[\{\beta\text{-}Fe_2GeW_{10}O_{37}(OH)_2\}_2]^{12-}$ (**2**), is structurally related to the reported tungstosilicate $[(\alpha\text{-}Fe_2SiW_{10}O_{37})_2(OH)_4]^{12-}$ and the tungstophosphate $[\alpha\text{-}Fe_4(OH)_4(PW_{10}O_{37})_2]^{10-}$. However, in **2**, the linkage of the two Keggin units is accomplished via iron centers located in the belt rather than in the cap. This allows for syn and anti isomers

(29) Keita, B.; Mbomekalle, I. M.; Nadjo, L.; Anderson, T. M.; Hill, C. L. *Inorg. Chem.* **2004**, *43*, 3257.

(30) Keita, B.; Mbomekalle, I. M.; Lu, Y-W.; Nadjo, L.; Berthet, P.; Anderson, T. M.; Hill, C. L. *Eur. J. Inorg. Chem.* **2004**, 3462.

of **1**, which might be present at 50% each in **CsKNa-2**. Both polyanions **1** and **2** were fully characterized in the solid state by FTIR, single-crystal X-ray diffraction, elemental analysis, and TGA.

The magnetic properties of **CsK-1** and **CsKNa-2** have been studied by magnetic susceptibility and magnetization measurements and fitted according to an isotropic exchange model. Both polyanions **1** and **2** exhibit diamagnetic ground states with a small amount of paramagnetic impurity.

The comparative electrochemical characterization of **1** and **2** was carried out at pH 5, close to the pH of their synthesis medium. As expected, the W^{VI} and Fe^{3+} waves are well separated. The splitting of the W^{VI} wave of **1** compared to the single W^{VI} wave of **2** is attributed to a difference in acid−base properties. Both polyanions have in common the simultaneous reduction of all of their Fe^{3+} centers, two in **1** and four in **2**. These waves are chemically reversible and electrochemically quasireversible, with a large potential difference between the cathodic and anodic waves. No splitting of the cathodic waves could be observed by raising the potential scan rate. For **2**, we observed an important pH effect on the potential location of the Fe^{3+} redox pattern. The shift is larger than usually observed for iron-substituted and multi-iron sandwich-type POMs. This behavior is tentatively attributed to the four hydroxo groups bridging the four Fe^{3+} centers in **2**.

Acknowledgment. U.K. thanks the German Research Council (DFG) for research funding (DFG-KO-2288/4-1). This work was also supported by the Jacobs University Bremen, the CNRS (UMR 8000), the Université Paris-Sud, and by the Spanish Ministerio de Educación y Ciencia (CTQ2005-09385-C03-01). Figures 1−4 were generated by *Diamond*, ver. 3.1e (copyright Crystal Impact GbR).

Supporting Information Available: Thermograms of **CsK-1** and **CsKNa-2**, UV−vis spectra of **1** and **2**, and X-ray crystallographic file in CIF format. This material is available free of charge via the Internet at http://pubs.acs.org.

IC701084X